Journal of Applied Geophysics 92 (2013) 1–7

Contents lists available at SciVerse ScienceDirect

Journal of Applied Geophysics

journal homepage: www.elsevier.com/locate/jappgeo

A generalized optimal 9-point scheme for frequency-domain scalar wave equation

Jing-Bo Chen *

Key Laboratory of Petroleum Resources Research, Institute of Geology and Geophysics, Chinese Academy of Sciences, P. O. Box 9825, Beijing 100029, China

ARTICLE INFO

Article history:
Received 18 September 2012
Accepted 4 February 2013
Available online 22 February 2013

Keywords:
Seismic numerical modeling
Directional derivative
Different directional intervals
Marmousi model

ABSTRACT

The rotated optimal 9-point scheme for frequency-domain scalar wave equation is widely used in frequency-domain full waveform inversion. This scheme requires equal directional sampling intervals, which limits its applicability. Recently, an average-derivative method was proposed to overcome this restriction. However, the average-derivative method is an algebraic approach, and therefore it does not inherit the geometrical property (coordinate transformations) of the rotated optimal 9-point scheme. In this paper, a geometrical approach is developed, and a generalized optimal 9-point scheme is constructed. This new scheme is based on a directional-derivative method, and includes the rotated optimal 9-point scheme as a special case. Like the average-derivative method, the number of grid points per wavelength is reduced from approximately 13 to approximately 4 by this new 9-point optimal scheme for both equal and unequal directional sampling intervals in comparison with the classical 5-point scheme. Unlike the average-derivative method, this generalized optimal 9-point scheme shares the geometrical property of the rotated optimal 9-point scheme.

1. Introduction

Recently, full waveform inversion (FWI) has been attracting a lot of attention in community of exploration geophysics. Generally speaking, FWI can be described as a full-wavefield-modeling-based data-fitting process to extract structural information of subsurface from seismograms (Virieux and Operto, 2009). FWI can be classified into two categories: time-domain FWI (Boonyasiriwat et al., 2009; Gauthier et al., 1986; Tarantola, 1984) and frequency-domain FWI (Pratt, 1999; Pratt and Worthington, 1990; Pratt et al., 1998).

Forward modeling is an important foundation of FWI. In the context of FWI, Pratt and Worthington (1990) developed the classical 5-point scheme for 2D frequency-domain scalar wave equation which imposes no restriction on directional sampling intervals. However, this scheme suffers from severe dispersion errors when large sampling intervals (4 points per smallest wavelength) are employed. To reduce the dispersion errors, very small sampling intervals (13 points per smallest wavelength) are required, which results in a significant increase of both storage requirements and CPU time.

Based on a rotated coordinate system, Jo et al. (1996) developed a 9-point operator to approximate the Laplacian and the mass acceleration terms. The coefficients of the 9-point operator are determined by obtaining the best normalized phase curves through an optimization process. Compared to the classical 5-point scheme developed by Pratt and Worthington (1990), this optimal 9-point scheme reduces the number of grid points per wavelength to less than 4, and leads to significant reductions of computer memory and CPU time. However, this optimal 9-point scheme loses the flexibility of the classical 5-point scheme because it requires equal directional sampling intervals (Jo et al., 1996).

To overcome the disadvantage of the rotated optimal 9-point scheme, Chen (2012) developed an average-derivative method. Unlike the method used by Jo et al. (1996), the average-derivative method does not need to use rotated coordinate system and only involves algebraic operations. In this paper, I will develop another approach to overcome the disadvantage of the rotated optimal 9-point scheme. This approach is based on the directional-derivative method proposed by Saenger et al. (2000). The directional-derivative method is closely related to the rotated-coordinate-system method, but has more flexibility.

In the next section, I will present the generalized optimal 9-point scheme based on the directional-derivative method and staggered-grid technique. This is followed by optimization of coefficients and a numerical dispersion analysis. Finally, I perform two numerical experiments on a homogenous model and the Marmousi model to test the generalized optimal 9-point scheme.

2. Generalized optimal 9-point scheme

Consider the two-dimensional scalar wave equation in frequency domain

$$\frac{\partial^2 P}{\partial x^2}+\frac{\partial^2 P}{\partial z^2}+\frac{\omega^2}{v^2}P=0, \tag{1}$$

* Tel.: +86 10 82998156.
E-mail address: chenjb@mail.iggcas.ac.cn.

0926-9851/$ – see front matter © 2013 Elsevier B.V. All rights reserved.
http://dx.doi.org/10.1016/j.jappgeo.2013.02.008

where P is the pressure wavefield, ω is the angular frequency, and $v(x,z)$ is the velocity.

The classical 5-point scheme for Eq. (1) is

$$\frac{P_{m+1,\,n}-2P_{m,\,n}+P_{m-1,\,n}}{\Delta x^2}+\frac{P_{m,\,n+1}-2P_{m,\,n}+P_{m,\,n-1}}{\Delta z^2}+\frac{\omega^2}{v_{m,\,n}^2}P_{m,\,n}=0, \tag{2}$$

where $P_{m,\,n}\approx P(m\Delta x,n\Delta z)$, and Δx and Δz are directional sampling intervals in the x-direction and z-direction, respectively.

As can be seen later (Section 3), within the phase velocity error of $\pm 1\%$, the classical 5-point scheme (2) requires approximately 13 grid points per shortest wavelength. In order to reduce numerical dispersion of the scheme (2), very fine grids are required. This leads to a huge amount of computer storage and CPU time. Therefore, reducing the number of grid points required per shortest wavelength is needed.

To this aim, a 9-point scheme for Eq. (1) was introduced by Jo et al. (1996):

$$\begin{aligned}&a\frac{P_{m+1,\,n}+P_{m-1,\,n}-4P_{m,\,n}+P_{m,\,n+1}+P_{m,\,n-1}}{\Delta^2}\\&+(1-a)\frac{P_{m+1,\,n+1}+P_{m-1,\,n+1}-4P_{m,\,n}+P_{m+1,\,n-1}+P_{m-1,\,n-1}}{2\Delta^2}\\&+\frac{\omega^2}{v^2}\left(cP_{m,\,n}+d\left(P_{m+1,\,n}+P_{m-1,\,n}+P_{m,\,n+1}+P_{m,\,n-1}\right)\right.\\&\left.+e\left(P_{m+1,\,n+1}+P_{m-1,\,n+1}+P_{m+1,\,n-1}+P_{m-1,\,n-1}\right)\right)=0,\end{aligned} \tag{3}$$

where $\Delta x=\Delta z=\Delta$. The constants a, c and d are weighting coefficients, and $e=\frac{1-c-4d}{4}$. For details, See Fig. 1a.

The rotated 9-point optimal scheme (3) with coefficients ($a=0.5461$, $c=0.6248$, and $d=0.0938$) reduces the number of grid points per shortest wavelength to less than 4, and results in remarkable reductions of computer storage and CPU time. However, this scheme has a requirement of $\Delta x=\Delta z$, which limits its application.

Now I try to develop a generalization of scheme (3) which is also valid for $\Delta x\neq\Delta z$. When $\Delta x\neq\Delta z$, the idea of rotated coordinate system can be developed into the directional-derivative method (Saenger et al., 2000). For details, see Fig. 1b. When $\Delta x\neq\Delta z$, the two directions l_1 and l_2 are not orthogonal to each other. One can compute directional-derivatives as follows:

$$\frac{\partial P}{\partial l_1}=\frac{\Delta x}{\Delta r}\frac{\partial P}{\partial x}-\frac{\Delta z}{\Delta r}\frac{\partial P}{\partial z}, \tag{4}$$

$$\frac{\partial P}{\partial l_2}=\frac{\Delta x}{\Delta r}\frac{\partial P}{\partial x}+\frac{\Delta z}{\Delta r}\frac{\partial P}{\partial z}, \tag{5}$$

where $\Delta r=\sqrt{\Delta x^2+\Delta z^2}$. From Eqs. (4) and (5), one can obtain

$$\frac{\partial^2 P}{\partial l_1^2}+\frac{\partial^2 P}{\partial l_2^2}=2\left(\frac{\Delta x}{\Delta r}\right)^2\frac{\partial^2 P}{\partial x^2}+2\left(\frac{\Delta z}{\Delta r}\right)^2\frac{\partial^2 P}{\partial z^2}, \tag{6}$$

$$\frac{\partial^2 P}{\partial l_1\partial l_2}=\left(\frac{\Delta x}{\Delta r}\right)^2\frac{\partial^2 P}{\partial x^2}-\left(\frac{\Delta z}{\Delta r}\right)^2\frac{\partial^2 P}{\partial z^2}. \tag{7}$$

From Eqs. (6) and (7), one can further obtain

$$\begin{aligned}\frac{\partial^2 P}{\partial x^2}+\frac{\partial^2 P}{\partial z^2}=&\left(\frac{\Delta r^2}{4\Delta x^2}+\frac{\Delta r^2}{4\Delta z^2}\right)\left(\frac{\partial^2 P}{\partial l_1^2}+\frac{\partial^2 P}{\partial l_2^2}\right)\\&+\left(\frac{\Delta r^2}{2\Delta x^2}-\frac{\Delta r^2}{2\Delta z^2}\right)\frac{\partial^2 P}{\partial l_1\partial l_2}.\end{aligned} \tag{8}$$

From Eq. (8), an approximation to the Laplacian can be obtained:

$$\begin{aligned}\frac{\partial^2 P}{\partial x^2}(m,n)+\frac{\partial^2 P}{\partial z^2}(m,n)=&\frac{P_{m+1,\,n+1}+P_{m-1,\,n+1}-4P_{m,\,n}+P_{m+1,\,n-1}+P_{m-1,\,n-1}}{2\tilde{\Delta}^2}\\&+\frac{\Delta z^2-\Delta x^2}{8\Delta x^2\Delta z^2}\left(P_{m+2,\,n}-P_{m,\,n+2}-P_{m,\,n-2}+P_{m-2,\,n}\right)\\&+\mathcal{O}\left((\Delta x,\Delta z)^2\right),\end{aligned} \tag{9}$$

where $\tilde{\Delta}=\frac{1}{\sqrt{\frac{1}{2}\left(\frac{1}{\Delta x^2}+\frac{1}{\Delta z^2}\right)}}$. $\tilde{\Delta}$ can be called the root-harmonic-mean-square interval of Δx and Δz (Chen, 2011).

Using Eq. (9), one can obtain the following scheme

$$\begin{aligned}&a\left[\frac{P_{m+1,\,n}-2P_{m,\,n}+P_{m-1,\,n}}{\Delta x^2}+\frac{P_{m,\,n+1}-2P_{m,\,n}+P_{m,\,n-1}}{\Delta z^2}\right]\\&+(1-a)\left[\frac{P_{m+1,\,n+1}+P_{m-1,\,n+1}-4P_{m,\,n}+P_{m+1,\,n-1}+P_{m-1,\,n-1}}{2\tilde{\Delta}^2}\right.\\&\left.+\frac{\Delta z^2-\Delta x^2}{8\Delta x^2\Delta z^2}\left(P_{m+2,\,n}-P_{m,\,n+2}-P_{m,\,n-2}+P_{m-2,\,n}\right)\right]\\&+\frac{\omega^2}{v^2}\left(cP_{m,\,n}+d\left(P_{m+1,\,n}+P_{m-1,\,n}+P_{m,\,n+1}+P_{m,\,n-1}\right)\right.\\&\left.+e\left(P_{m+1,\,n+1}+P_{m-1,\,n+1}+P_{m+1,\,n-1}+P_{m-1,\,n-1}+A\right)\right)=0.\end{aligned} \tag{10}$$

where

$$A=\begin{cases}0, & \Delta x=\Delta z,\\ P_{m+2,\,n}-P_{m,\,n+2}-P_{m,\,n-2}+P_{m-2,\,n}, & \Delta x\neq\Delta z.\end{cases}$$

Scheme (10) is a 13-point scheme. Compared to the rotated optimal 9-point scheme, it includes four additional grid points. This is caused by the second-order mixed partial derivative in Eq. (8). When $\Delta x=\Delta z$, the term involving the mixed partial derivative becomes zero, and the 13-point scheme becomes the rotated optimal 9-point scheme.

On the other hand, without the condition of $\Delta x=\Delta z$, the scheme (10) can be simplified too. Using a staggered-grid technique (Štekl and Pratt, 1998), the second term on the right-hand side of Eq. (8) can be discretized as follows:

$$\left(\frac{\Delta r^2}{2\Delta x^2}-\frac{\Delta r^2}{2\Delta z^2}\right)\frac{\partial^2 P}{\partial l_1\partial l_2}\approx\frac{\Delta z^2-\Delta x^2}{2\Delta x^2\Delta z^2}\left(P_{m+1,\,n}-P_{m,\,n+1}-P_{m,\,n-1}+P_{m-1,\,n}\right). \tag{11}$$

Using the approximation (11), the 13-point scheme (10) can be simplified into a 9-point scheme:

$$\begin{aligned}&a\left[\frac{P_{m+1,\,n}-2P_{m,\,n}+P_{m-1,\,n}}{\Delta x^2}+\frac{P_{m,\,n+1}-2P_{m,\,n}+P_{m,\,n-1}}{\Delta z^2}\right]\\&+(1-a)\left[\frac{P_{m+1,\,n+1}+P_{m-1,\,n+1}-4P_{m,\,n}+P_{m+1,\,n-1}+P_{m-1,\,n-1}}{2\tilde{\Delta}^2}\right.\\&\left.+\frac{\Delta z^2-\Delta x^2}{2\Delta x^2\Delta z^2}\left(P_{m+1,\,n}-P_{m,\,n+1}-P_{m,\,n-1}+P_{m-1,\,n}\right)\right]\\&+\frac{\omega^2}{v^2}\left(cP_{m,\,n}+d\left(P_{m+1,\,n}+P_{m-1,\,n}+P_{m,\,n+1}+P_{m,\,n-1}\right)\right.\\&\left.+e\left(P_{m+1,\,n+1}+P_{m-1,\,n+1}+P_{m+1,\,n-1}+P_{m-1,\,n-1}\right)\right)=0.\end{aligned} \tag{12}$$

The scheme (12) is a generalized optimal 9-point scheme because it includes the rotated optimal 9-point scheme (3) as a special case

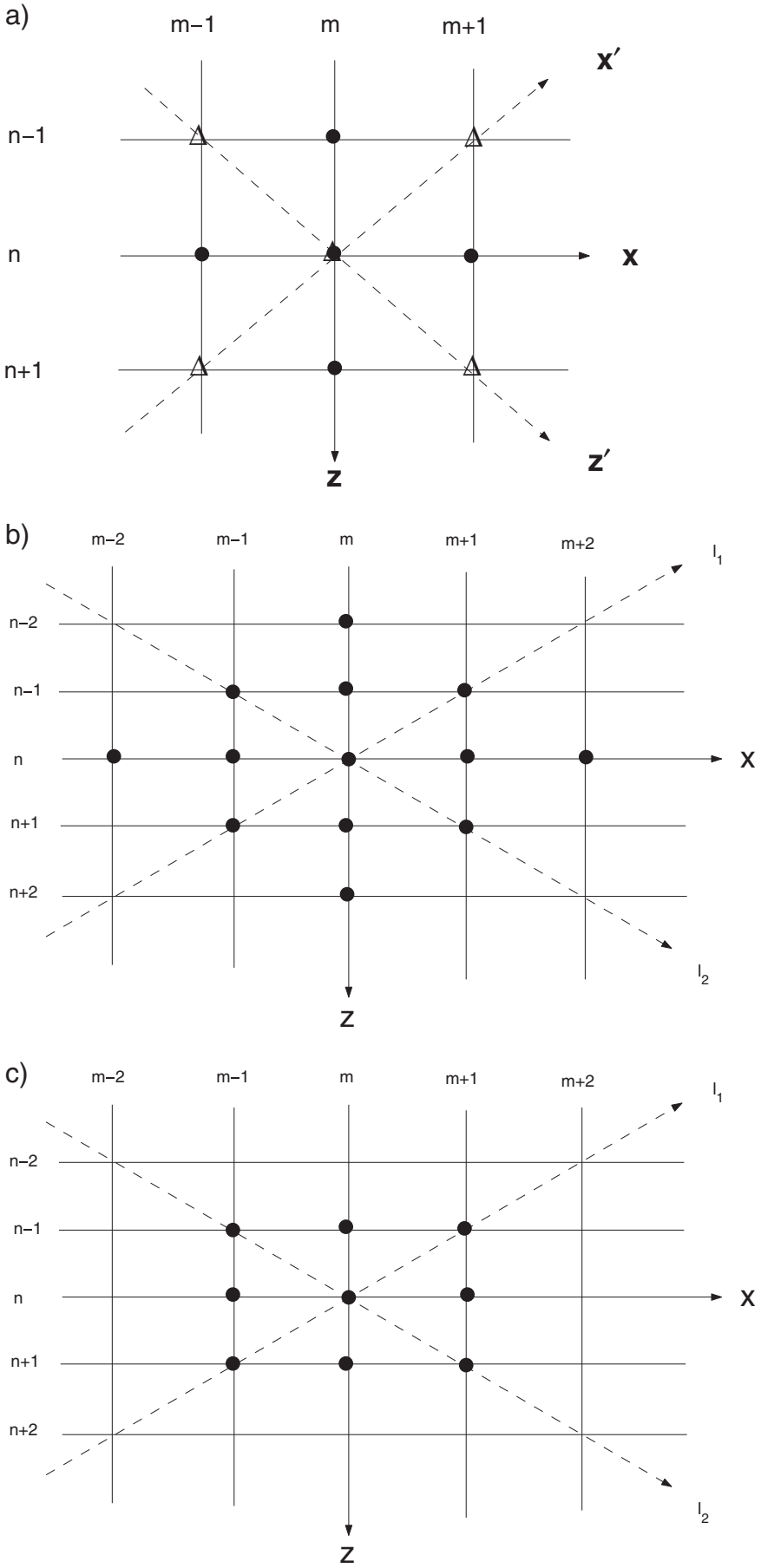

Fig. 1. Schematic of the rotated optimal 9-point scheme (a), the 13-point optimal scheme (b), and the generalized optimal 9-point scheme (c).

when $\Delta x = \Delta z$. In addition, the scheme (12) also includes the classical 5-point scheme (2) as a special case when $a = 1$, $c = 1$, and $d = 0$.

3. Optimization and dispersion analysis

In this section, I perform optimization of the coefficients in the generalized 9-point scheme (12), and then make dispersion analysis.

Substituting $P(x,z,\omega) = P_0 e^{i(k_x x + k_z z)}$ into Eq. (12), one obtains the discrete dispersion relation

$$\frac{\omega^2}{v^2} = \frac{2a\left[(1-E_x) + r^2(1-E_z)\right] + (1-a)\left[\left(r^2+1\right)(1-E_xE_z) + \left(r^2-1\right)(E_x-E_z)\right]}{\Delta x^2[c + 2d(E_x+E_z) + 4eE_xE_z]}, \tag{13}$$

where $r = \frac{\Delta x}{\Delta z}$, $E_x = \cos(k_x\Delta x)$, and $E_z = \cos(k_z\Delta z)$. Here, I first consider the case $\Delta x \geq \Delta z$.

From Eq. (13), the normalized phase velocity can be derived as follows

$$\frac{V_{ph}}{v} = \frac{\left\{2a\left[(1-E_x) + r^2(1-E_z)\right] + (1-a)\left[\left(r^2+1\right)(1-E_xE_z) + \left(r^2-1\right)(E_x-E_z)\right]\right\}^{\frac{1}{2}}}{\frac{2\pi}{G}[c + 2d(E_x+E_z) + 4eE_xE_z]^{\frac{1}{2}}}, \tag{14}$$

where V_{ph} is the phase velocity and

$$E_x = \cos(k_x\Delta x) = \cos\left(\frac{2\pi \sin\theta}{G}\right), \quad E_z = \cos\left(\frac{2\pi \cos\theta}{Gr}\right),$$

where $k_x = k\sin\theta$, $k_z = k\cos\theta$, and $G = \frac{2\pi}{k\Delta x}$.

The coefficients a, c, and d are determined by minimizing the phase error:

$$E(a,c,d) = \int\int \left[1 - \frac{V_{ph}\left(\theta, \tilde{k}; a, c, d\right)}{v}\right]^2 d\ \tilde{k} d\ \theta, \tag{15}$$

where $\tilde{k} = \frac{1}{G}$.

The ranges of $\tilde{k}$ and θ are taken as [0,0.25] and $[0, \frac{\pi}{2}]$, respectively. A constrained nonlinear optimization program fmincon in Matlab is used to solve the optimization problem (15). The optimization coefficients for different $r = \frac{\Delta x}{\Delta z}$ are listed in Table 1. One can see that the coefficient a varies with $\frac{\Delta x}{\Delta z}$, and the changes in coefficients c and d are small.

Now I perform numerical dispersion analysis. Fig. 2 shows the normalized phase velocity curves of the classical five-point scheme (2) and the generalized optimal 9-point scheme (12) for different $\frac{\Delta x}{\Delta z}$ when $\Delta x \geq \Delta z$. The propagation angles are taken from 0° to 90° with an increment of 15°. From this figure, one can conclude that within the phase error of $\pm 1\%$, the classical five-point scheme (2) requires approximately 13 grid points (precisely 12.8) per shortest wavelength, while the generalized optimal 9-point scheme (12) requires approximately 4 points (precisely 3.6 points) for all ratios of directional sampling intervals.

Table 1
Optimization coefficients for a, c, and d for different $\frac{\Delta x}{\Delta z}$ when $\Delta x \geq \Delta z$.

	a	c	d
$\frac{\Delta x}{\Delta z} = 1$	0.588786	0.634826	0.091293
$\frac{\Delta x}{\Delta z} = 2$	0.604417	0.636103	0.090974
$\frac{\Delta x}{\Delta z} = 3$	0.611502	0.635736	0.091071
$\frac{\Delta x}{\Delta z} = 4$	0.615393	0.635805	0.091049

When $\Delta z > \Delta x$, one should define G as $G = \frac{2\pi}{k\Delta z}$, and then the same optimization process can be made. The optimization coefficients for the case of $\Delta z > \Delta x$ are listed in Table 2. For the case of $\Delta z > \Delta x$, the same conclusions on dispersion can be drawn.

4. Numerical examples

In this section, I present two numerical examples to verify the theoretical analysis on the classical 5-point scheme (2) and the generalized optimal 9-point scheme.

The first numerical example is about a homogeneous velocity model with a velocity of 3000 m/s (Fig. 3). Analytical solution can be obtained in this case to make comparisons with the numerical solutions. Horizontal and vertical samplings are $nx = 101$ and $nz = 41$, respectively. A Ricker wavelet with a peak frequency of 25 Hz is placed at the center of the model as a source, and a receiver is set 25 samples away from the source horizontally. The maximum frequency used in the modeling is 70 Hz. According to the criterion of 4 grid points per smallest wavelength, horizontal sampling interval is determined by $dx = 3000/70/4$ m ≈ 11 m. Vertical sampling interval is taken as $dz = dx/2$. For this ratio of directional sampling intervals, the optimization coefficients of the scheme (12) is $a = 0.604417$, $c = 0.636103$, and $d = 0.090974$.

For the homogeneous model, the analytical solution can be obtained as (Alford et al., 1974):

$$P(x,z,t) = i\pi\mathcal{F}^{-1}\left[H_0^{(2)}\left(\frac{\omega}{v}r\right)\mathcal{F}(f(t))\right], \tag{16}$$

where $\mathcal{F}$ and $\mathcal{F}^{-1}$ are forward and inverse Fourier transformations with respect to time, respectively, $f(t)$ is the Ricker wavelet, $H_0^{(2)}$ is the second Hankel function of order zero, and $r = \sqrt{(x-x_0)^2 + (z-z_0)^2}$. Here (x_0, z_0) is the source position.

Fig. 4 depicts the results computed with the analytical formula (16), the classical 5-point scheme (2) and the generalized optimal 9-point scheme (12), respectively. From the figure, one can see that the simulation result with the generalized optimal 9-point scheme (12) agrees well with the analytical result while the result computed with the classical 5-point scheme (2) exhibits discrepancies due to the numerical dispersion.

Second, I consider a more realistic model. Fig. 5a shows the Marmousi model. Horizontal and vertical samplings are $nx = 737$ and $nz = 751$, respectively. The sampling intervals of the Marmousi model are $dx = 12.5$ m and $dz = 4$ m. For this ratio of directional sampling intervals, the optimization coefficients of the generalized optimal 9-point scheme (12) is $a = 0.612116$, $c = 0.635714$, and $d = 0.091071$. A Ricker wavelet with peak frequency of 15 Hz is placed at ($x = 4600$ m, $z = 1500$ m) as a source which is marked by a star. Absorbing boundary conditions with 45-degree one-way equation are used at the four sides of the model. Fig. 5b and c shows the 15-Hz and 30-Hz monochromatic wavefields, respectively. No visible dispersion and boundary reflections can be found. For the Marmousi model, the rotated optimal 9-point scheme cannot be applied due to the fact of $dx \neq dz$, but the generalized optimal 9-point scheme is still valid due to its flexibility.

5. Discussions

The average-derivative method (Chen, 2012) and the directional-derivative method developed in this paper both generalize the rotated optimal 9-point scheme. The average-derivative method is more general, and the directional-derivative possesses the geometrical property. In terms of accuracy, the average-derivative method is slightly higher than

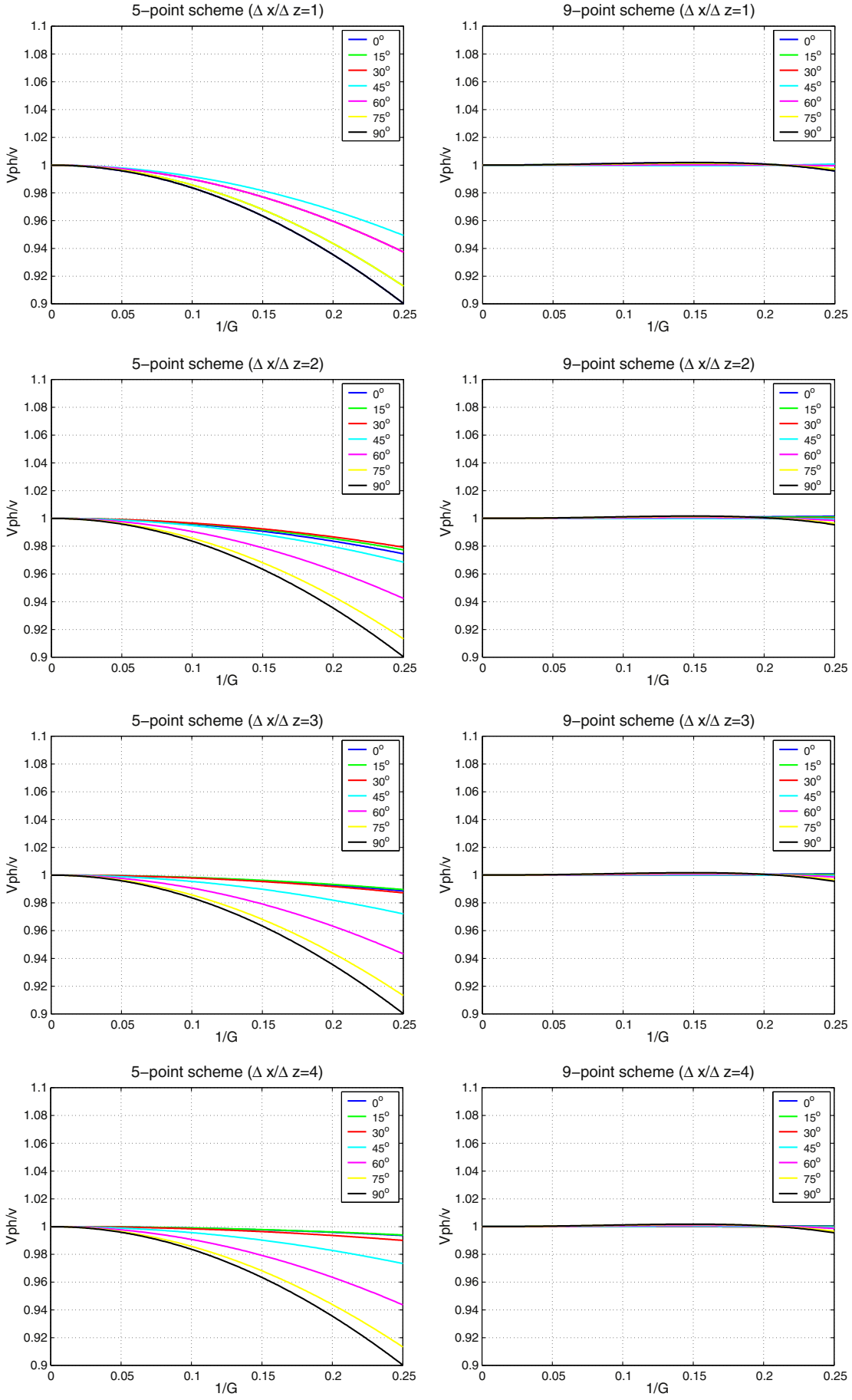

Fig. 2. Normalized phase velocity curves of the classical five-point scheme and the generalized optimal 9-point scheme for different $\frac{\Delta x}{\Delta z}$ when $\Delta x \geq \Delta z$.

Table 2
Optimization coefficients for a, c, and d for different $\frac{\Delta z}{\Delta x}$ when $\Delta x<\Delta z$.

	a	c	d
$\frac{\Delta z}{\Delta x}=2$	0.604417	0.636103	0.090974
$\frac{\Delta z}{\Delta x}=3$	0.611502	0.635736	0.091071
$\frac{\Delta z}{\Delta x}=4$	0.615393	0.635805	0.091049

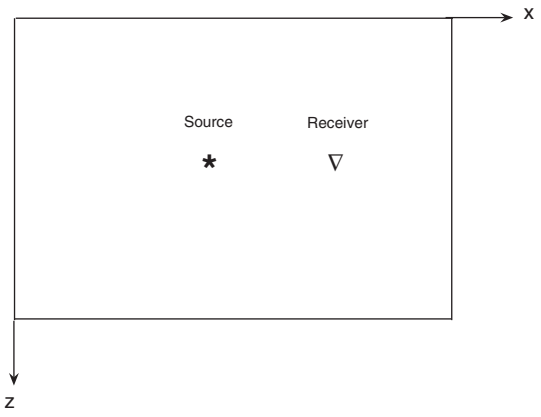

Fig. 3. Schematic of the homogeneous model.

the directive–derivative method. When considering the geometrical property, the directional-derivative method is a better choice.

The directive–derivative method can be generalized to the 3D case by using the coordinate transformations developed in Operto et al. (2007). In addition, for a time-domain wave equation, its discretization involves both temporal and spatial discretization. Therefore, the generalized optimal 9-point scheme (12) can be easily adapted to obtain a time-domain scheme:

$$\begin{aligned} & a\left[\frac{P^l_{m+1,\,n}-2P^l_{m,\,n}+P^l_{m-1,\,n}}{\Delta x^2}+\frac{P^l_{m,\,n+1}-2P^l_{m,\,n}+P^l_{m,\,n-1}}{\Delta z^2}\right] \\ & +(1-a)\left[\frac{P^l_{m+1,\,n+1}+P^l_{m-1,\,n+1}-4P^l_{m,\,n}+P^l_{m+1,\,n-1}+P^l_{m-1,\,n-1}}{2\tilde{\Delta}^2}\right. \\ & \left.+\frac{\Delta z^2-\Delta x^2}{2\Delta x^2\Delta z^2}\left(P^l_{m+1,\,n}-P^l_{m,\,n+1}-P^l_{m,\,n-1}+P^l_{m-1,\,n}\right)\right] \\ & -\frac{1}{v^2}\frac{P^{l+1}_{m,\,n}-2P^l_{m,\,n}+P^{l-1}_{m,\,n}}{\Delta t^2}=0, \end{aligned} \tag{17}$$

where $P^l_{m,\,n}\approx P(m\Delta x,n\Delta z,l\Delta t)$, and Δt is the time-step size.

6. Conclusions

Based on the directional-derivative approach, I have presented a generalized optimal 9-point scheme which overcomes the disadvantage of the rotated optimal 9-point scheme by removing the requirement of equal directional sampling intervals. In addition, this new scheme inherits the geometrical property of the rotated optimal 9-point scheme. Compared to the classical 5-point scheme, the number of grid points per wavelength is reduced from approximately 13 to approximately 4 by this new 9-point optimal scheme for both equal and unequal directional sampling intervals. Two numerical examples demonstrate the greater accuracy and flexibility of the generalized optimal 9-point scheme.

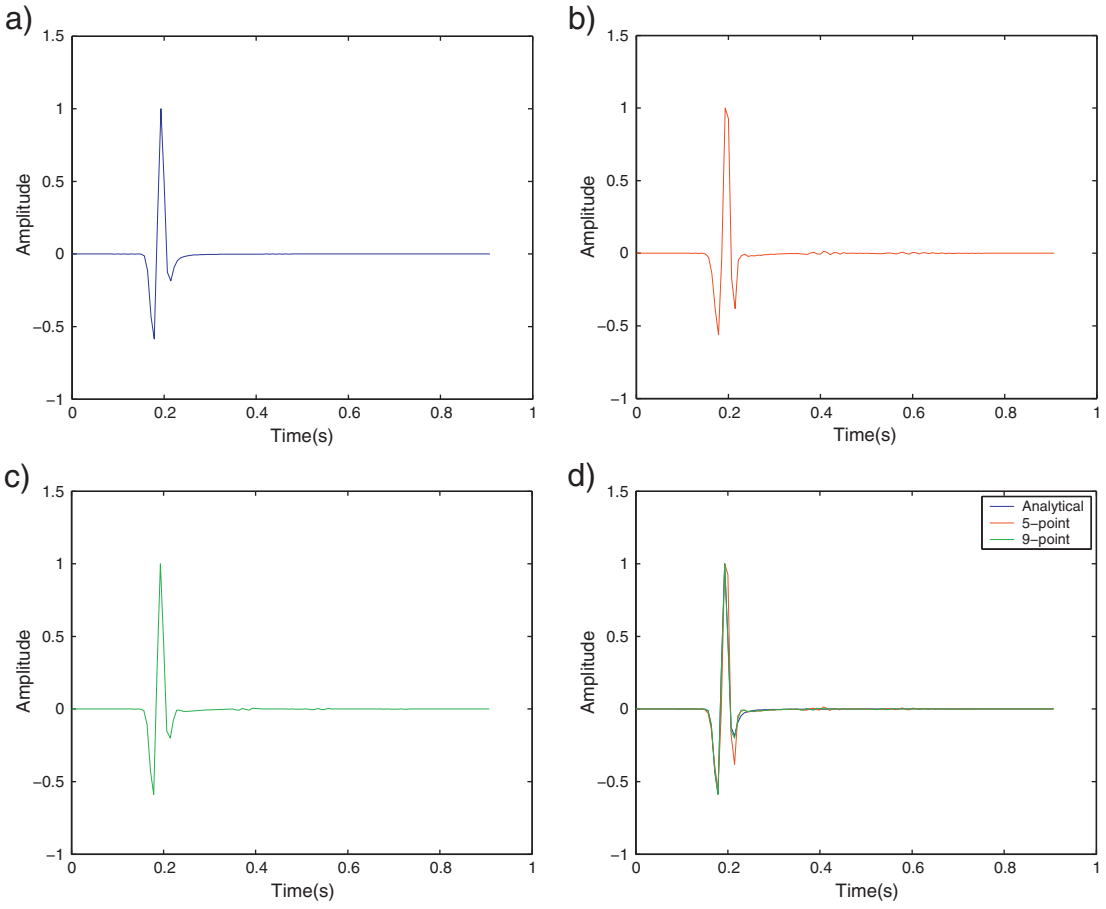

Fig. 4. Seismograms computed with the analytical method (a), the classical five-point scheme (b), the generalized optimal 9-point scheme (c) and the superimposed results (d).

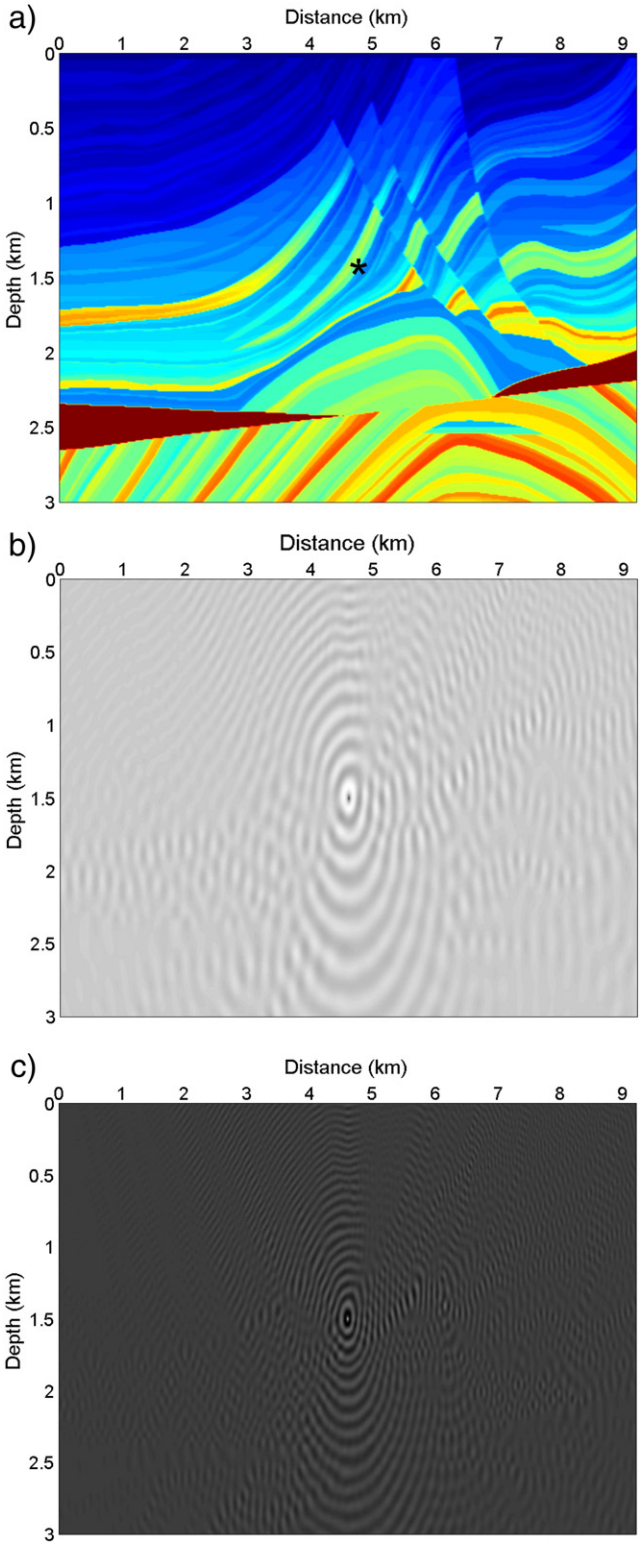

Fig. 5. Marmousi model (a), and the 15-Hz (b) and 30-Hz (c) monochromatic wavefields computed with the generalized optimal 9-point scheme.

Acknowledgments

This work is supported by the National Natural Science Foundation of China under grant nos. 41274139 and 40974074.

References

Alford, R.M., Kelly, K.R., Boore, D.M., 1974. Accuracy of finite-difference modeling of the acoustic wave equation. Geophysics 39 (6), 834–842.
Boonyasiriwat, C., Valasek, P., Routh, P., Cao, W., Schuster, G.T., Macy, B., 2009. An efficient multiscale method for time-domain waveform tomography. Geophysics 74 (6), WCC59–WCC68.
Chen, J.-B., 2011. A stability formula for Lax–Wendroff methods with fourth-order in time and general-order in space for the scalar wave equation. Geophysics 76 (2), T37–T42.
Chen, J.-B., 2012. An average-derivative optimal scheme for frequency-domain scalar wave equation. Geophysics 77 (6), T201–T210.
Gauthier, O., Virieux, J., Tarantola, A., 1986. Two-dimensional nonlinear inversion of seismic waveforms. Geophysics 51, 1387–1403.
Jo, C.-H., Shin, C., Suh, J.H., 1996. An optimal 9-point, finite-difference, frequency-space, 2-D scalar wave extrapolator. Geophysics 529–537.
Operto, S., Virieux, J., Amestoy, P., L'Excellent, J.-Y., Giraud, L., Ali, H.B.H., 2007. 3D finite-difference frequency-domain modeling of visco-acoustic wave propagation using a massively parallel direct solver: a feasibility study. Geophysics 72 (5), SM195–SM211.
Pratt, R.G., 1999. Seismic waveform inversion in the frequency domain, Part I: theory and verification in a physical scale model. Geophysics 64, 888–901.
Pratt, R.G., Worthington, M.-H., 1990. Inverse theory applied to multi-source cross-hole tomography, part I: acoustic wave-equation method. Geophysical Prospecting 38, 287–310.
Pratt, R.G., Shin, C., Hicks, G.J., 1998. Gauss–Newton and full Newton methods in frequency-space seismic waveform inversion. Geophysical Journal International 133, 341–362.
Saenger, E.H., Gold, N., Shapiro, S.A., 2000. Modeling the propagation of elastic waves using a modified finite-difference grid. Wave Motion 31, 77–92.
Štekl, I., Pratt, R.G., 1998. Accurate visoelastic modeling by frequency-domain finite difference using rotated operators. Geophysics 63, 1779–1794.
Tarantola, A., 1984. Inversion of seismic reflection data in the acoustic approximation. Geophysics 49, 1259–1266.
Virieux, J., Operto, S., 2009. An overview of full-waveform inversion in exploration geophysics. Geophysics 74 (6), WCC1–WCC26.